Transformation of a single-photon field into bunches of pulses

R. N. Shakhmuratov,[1,2] F. G. Vagizov,[1,2,3] V. A. Antonov,[2,4,5] Y. V. Radeonychev,[4,5]
Marlan O. Scully,[3] and Olga Kocharovskaya[3]
[1]*Kazan Physical-Technical Institute, Russian Academy of Sciences, 10/7 Sibirsky Trakt, Kazan 420029, Russia*
[2]*Kazan Federal University, 18 Kremlyovskaya Street, Kazan 420008, Russia*
[3]*Institute for Quantum Studies and Engineering and Department of Physics and Astronomy, TAMU, College Station, Texas 77843-4242, USA*
[4]*Institute of Applied Physics of the Russian Academy of Sciences, Nizhny Novgorod 603950, Russia*
[5]*N. I. Lobachevsky State University of Nizhny Novgorod, Nizhny Novgorod, 603950, Russia*
(Received 26 March 2015; published 19 August 2015)

We propose a method to transform a single-photon field into bunches of pulses with controllable timing and number of pulses in a bunch. The method is based on transmission of a photon through an optically thick single-line absorber vibrated with a frequency appreciably exceeding the width of the absorption line. The narrow spectrum of the incoming photon is "seen" by the vibrated absorber as a comb of equidistant spectral components separated by the vibration frequency. Tuning the absorber in resonance with mth spectral component transforms the output radiation into bunches of pulses with m pulses in each bunch. We provide a simple analytical solution clearly describing this effect and experimentally demonstrate the proposed technique with a single 14.4-keV photon and an ensemble of vibrated ^{57}Fe nuclei. This method opens an alternate way to the production of time-bin qubits.

DOI: 10.1103/PhysRevA.92.023836 PACS number(s): 42.50.Gy

I. INTRODUCTION

γ-photon–nuclear ensemble interfaces represent an interesting alternative to optical photon–atomic ensemble interfaces and the useful platform for testing new techniques. It is interesting to point out that in spite of the short wavelength of the γ photon, its coupling with an ensemble of resonant nuclei, incorporated into room-temperature solid, can be made much more efficient than the coupling of optical photon with an ensemble of atoms. It is due to unique combination of high solid-state density with a very narrow, typically, lifetime broadened spectral lines of recoilless Mössbauer transitions, even at room temperature. As a result, optical thickness of the order of one can be realized at extremely small physical thicknesses of the order of 100 nm. Due to this fact, many coherent cooperative effects such as cooperative forward scattering, dynamical beats, single-photon superradiance, collective Lamb shift, etc., have been widely studied in γ optics [1–6]. The further advantages are an existence of natural radioactive sources of heralded single γ photons due to the cascade decay of one nucleus during coherence time of the photon of interest, high efficiency of γ-photon detectors, potentially sub-Å focusing, and large capacity of the information channels.

Recent fundamental and technological breakthroughs in hard x-ray/γ-ray optics, including development of bright coherent x-ray free-electron lasers (XFELs) based sources [7], high-efficient back-reflecting mirrors, waveguides, and cavities [8–10], nanometer focusing facilities [11], and efficient beam splitters [12], stimulate to extension of quantum optics to quantum γ-ray optics [13–18] and quantum electronics to quantum "nucleonics" [19].

The particular problem, addressed in this work, is a temporal shaping of a single γ photon, including formation of the single and multiple peak waveforms, required for preparation of time-bin qubits and qudits and for realization of quantum memories [20,21]. The techniques, developed for shaping of single optical photons and for time-bin qubits preparation, include transmission of photons, produced by parametric down conversion, through unbalanced interferometers [22–24], temporally modulated pumping of a single atom in a QED cavity [25], and using of electro-optical amplitude modulator, activated by detection of one photon from the time-energy entangled biphoton pair [26]. Such techniques are currently not available in the γ domain.

The efficient control of the waveforms of single γ photons via vibration of the single-line absorber, which results in phase modulation of its interaction with the radiation field due to the Doppler effect and production of the vibrational sidebands, has been demonstrated very recently in our work [14]. In particular, the trains of single pulses with high-peak intensities and duration much shorter than the duration of the incoming photon were produced by tuning the absorber into resonance with the first Stokes or anti-Stokes vibrational sideband, whose intensity was maximized by choosing proper amplitude of the mechanical vibration of the absorber. In this work, we extend and generalize our first results. Namely, we show that tuning the incoming photon in resonance with a particular sideband $\omega_a \pm m\Omega$, maximized by proper choice of the vibration amplitude, results in splitting of a single-photon pulse into a train of bunched pulses, where ω_a is a resonant frequency of the single-line absorber and Ω is the vibration frequency. Each bunch contains m pulses. Bunches are separated by the dark windows. Both bunches and dark windows have equal duration coinciding with the half of the period of the mechanical vibrations. Full width at half maximum of each pulse in a bunch can be roughly estimated as $T_{\rm vib}/4m$, where $T_{\rm vib} = 2\pi/\Omega$ is the mechanical vibration period. Therefore, the duration of the pulses shortens m times with increase of m. We derived a simple analytical solution explaining the formation of such pulse-bunched single photons.

We show that single-photon pulse bunching opens a way of producing qudits in γ optics, which is different from other ways reported in optics.

 ©2015 American Physical Society

We demonstrate our proposal in the γ domain where single photons are emitted by a naturally decaying radioactive ^{57}Co nuclei. They are ideal for test experiments since the coherence length of emitted photons is very long and simple electronics can be used. The sources containing these nuclei are commercially available and relatively cheap. They emit 14.4-keV photons with the rate 1000–5000 s^{-1} ensuring that during the coherence time of the photon (141 ns), we may have no more than only one photon. Moreover, detectors in the γ domain have high quantum efficiency and almost no dark counts. In our experiment, a 14.4-keV photon of long coherence length (42 m) and duration of hundreds of nanoseconds is split in time bins by transmission through a vibrating single-line absorber whose physical thickness (25 μm) is more than a million times shorter than the coherence length of a photon.

We note that other techniques, developed in the γ domain, such as magnetic switching [15,17,27–29], stepwise phase modulation of the radiation field [30–38], ultrasonic modulation [39], and cooperative emission in planar waveguides [10], can be also used to perform photon shaping. They could extend standard optical methods of quantum information processing.

II. BASIC IDEA

A single photon, emitted by a source nucleus, has a Lorenzian spectrum whose width is mainly defined by the lifetime of the nuclear excited state. We transmit such a photon through a thick resonant absorber with a single resonance line having approximately the same width as the spectrum of the radiation field. The absorber experiences periodic mechanical vibrations along the photon propagation direction. They are induced by the piezoelectric transducer.

In the reference frame of the pistonlike vibrating absorber, the incident field phase oscillates as $(2\pi\delta/\lambda)\sin\Omega t$, where Ω and δ are the frequency and amplitude of the periodical displacements, λ is the wavelength of the incident radiation field. The probability amplitude of the radiation field in the laboratory reference frame $a_L(t,z) = a_0(t)\exp(-i\omega_s t + ik_s z)$ is transformed to $a_A(t,z') = a_L(t,z')\exp[ip\sin(\Omega t+\varphi)]$ in the vibrating absorber reference frame. Here, ω_s, k_s are the frequency and wave number of the radiation field, z and $z' = z + \delta\sin(\Omega t+\varphi)$ are coordinates in the laboratory and vibrating reference frames along photon propagation direction $\mathbf{z}$, $p = 2\pi\delta/\lambda$ is the modulation index, and φ is the phase of the absorber vibration.

The probability amplitude $a_A(t,z)$ can be expressed as

$$a_A(t,z') = a_L(t,z')\sum_{m=-\infty}^{+\infty} J_m(p)e^{im(\Omega t+\varphi)}, \quad (1)$$

where $J_m(p)$ is the Bessel function of the mth order. From this expression, it is clear that the vibrating absorber "sees" the incident radiation field as an equidistant frequency comb with spectral components $\omega_s - m\Omega$ having Lorenzian shapes and intensities, which are proportional to $J_m^2(p)$.

Let us say that the mth component of this field is tuned in resonance with the absorber. If the half-width of the components γ_s [defined by the half-width of the spectrum of the incident field $a_L(t,z)$] is much smaller than the distance between neighboring components Ω, then we may assume that only the resonant component interacts with the absorber and others pass through without interaction. Within the adopted approximation, only the interacting component is coherently scattered by nuclei of the absorber.

For a weak field, the output radiation can be expressed as a sum of the incident and coherently scattered radiation fields [40]. In the case of a resonant single-line radiation these fields interfere destructively, resulting in radiation damping. For the frequency comb, only the resonant component is coherently scattered by resonant nuclei and the scattered field interferes with the whole frequency comb at the exit of the absorber. Therefore, the output radiation field reveals unusual properties.

The shape of a single photon wave packet is described by the exponentially decaying function with the rate γ_s:

$$a_L(t-t_0) = \Theta(t-t_0)\exp[-(i\omega_s+\gamma_s)(t-t_0)+ik_s z], \quad (2)$$

where $\Theta(t-t_0)$ is the Heaviside step function and t_0 is the moment of time when the excited state of the source nucleus is formed. Such a shape is typical for single-photon wave packets if the time of formation of the excited-state particle, producing this single photon, is known (see, for example, Refs. [41,42]). In our experiments, the source nucleus ^{57}Co decays by electron capture to ^{57m}Fe, which decays in turn by emission of a 122-keV photon, followed by a 14.4-keV photon to the ground state ^{57}Fe. In this cascade decay the detection of the 122-keV photon heralds the formation of a 14.4-keV excited state of the ^{57}Fe nucleus in the source (see, for example, Ref. [41]). The absorber contains ground state ^{57}Fe nuclei resonant for 14.4-keV photons.

The propagation of the field [Eq. (2)] through a single-line resonant absorber (not vibrating) can be described classically [41] or quantum mechanically [43]. The result is well known in γ domain [41,43] and in quantum optics [44]. In the simplest case, if $\omega_s = \omega_a$ and $\gamma_s = \gamma_a$, where ω_a and γ_a are the resonant frequency and half-width of the absorption line of the absorber, respectively, the output probability amplitude is

$$a_{\rm out}(t,l) = a_L(t,l)J_0(2\sqrt{bt}), \quad (3)$$

where $t_0 = 0$ and l is the physical thickness of the absorber. Here and in the following, we disregard retardation effects $t - l/c \approx t$ since the physical length of the absorber is small and retardation time l/c is short with respect to the time scale of the amplitude evolution. The parameter $b = \gamma_a T_a/2$ depends on the optical depth of the absorber, which is $T_a = \alpha_B l$, where $\alpha_B = N\sigma$ is the Beer's law absorption coefficient, N is the density of ^{57}Fe nuclei in the absorber, and σ is the resonant cross section. Here, we disregard recoil processes in nuclear absorption and emission assuming that recoilless fraction (Debye-Waller factor) is $f_a = 1$. These processes will be taken into account in data analysis.

Since we are interested only in the detection probability of a photon, which is equivalent to the radiation intensity, the cases when the absorber vibrates with respect to the source at rest or vice versa give the same result. For simplicity, we consider the case of the vibrating source. Then, the radiation field at the exit of the absorber at rest is the sum of the incident comb, Eq. (1) with $z' \to z$, and the coherently scattered field.

We suppose that the frequency component $\omega_s - m\Omega$ is in resonance with the absorber. Then, according to Eq. (3), the probability amplitude of the coherently scattered field is

$$a_{\rm sct}(t,l) = a_L(t,l)S_m(t)e^{im(\Omega t+\varphi)}, \tag{4}$$

where $S_m(t) = J_m(p)[J_0(2\sqrt{bt}) - 1]$. This field is just the output field $a_{\rm out}(t,l)$ for the component $a_L(t,z)J_m(p)\exp[im(\Omega t+\varphi)]$ minus this component if it would propagate without interaction with the absorber [35,45]. Simple calculation of the probability $P(t) = |a_A(t,l) + a_{\rm sct}(t,l)|^2$ of the output radiation field gives

$$P(t) = \Theta(t)e^{-2\gamma t}\left[1 + 2S_m(t)\cos\psi_m(t) + S_m^2(t)\right], \tag{5}$$

where $\gamma = \gamma_a = \gamma_s$ and $\psi_m(t) = m(\Omega t+\varphi) - p\sin(\Omega t + \varphi)$. Time evolution of the probability $P(t)$ for $m = 1$, 2, and 3 is shown in Figs. 1(a), 1(b), and 1(c), respectively, where

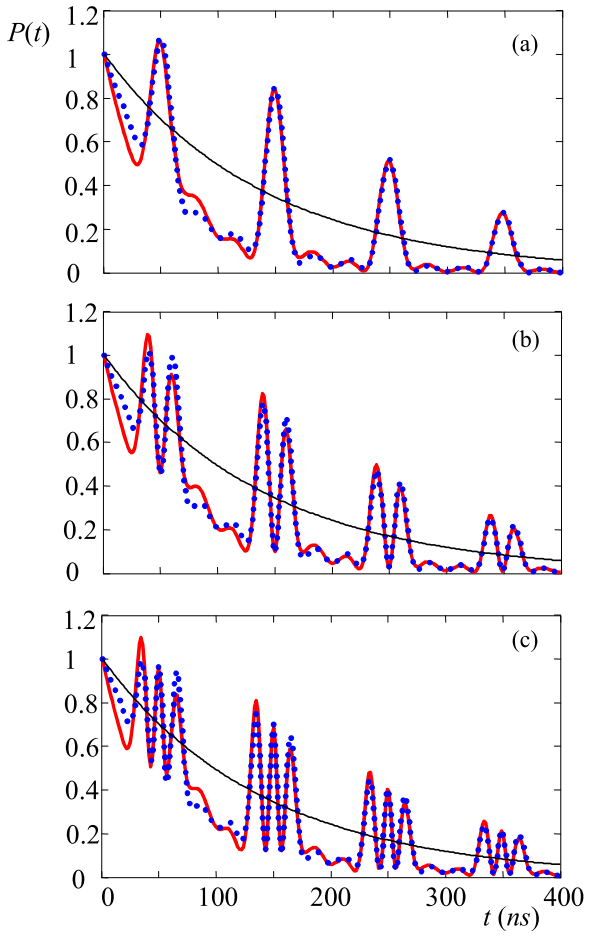

FIG. 1. (Color online) Time dependence of the detection probability of a photon $P(t)$ at the exit of the absorber vibrating with the frequency $\Omega = 10$ MHz and phase $\varphi = 0$. Optical thickness of the absorber is $T_a = 5.2$ and $\gamma_a = \gamma_s = 1.13$ MHz. The frequency of the radiation field ω_s is tuned in resonance with the first sideband $\omega_a + \Omega$ (a), the second sideband $\omega_a + 2\Omega$ (b), and the third sideband $\omega_a + 3\Omega$ (c). The value of the modulation index is taken optimal in each case, i.e., $p_1 = 1.8$ (a), $p_2 = 3.1$ (b), and $p_3 = 4.2$ (c) (see the text). Dotted line (in blue) corresponds to the analytical approximation (5), solid line (in red) demonstrates the result obtained from the exact solution (6), and thin solid line (in black) shows exponential decay of the single-photon wave packet [Eq. (2)].

the results of approximate Eq. (5) are compared with the exact expression $P_{\rm ext}(t) = |a_{\rm ext}|^2$, which is obtained if we calculate the probability amplitude without any assumptions (see, for example, Ref. [33]), i.e.,

$$a_{\rm ext}(t,l) = a_A(t,l) - b\int_0^t a_A(t-\tau,l)j_1(b\tau)e^{-\gamma_a\tau - i\omega_a\tau}d\tau, \tag{6}$$

where $j_1(b\tau) = J_1(2\sqrt{b\tau})/\sqrt{b\tau}$. Small misfits can be almost excluded if we take into account the contribution of the two neighboring satellites, both red and blue detuned from the resonant component of the comb (see Appendix A).

We see that the shape of the photon wave packet is transformed into bunches of pulses with m pulses in a bunch. The pulses are produced due to constructive interference of the incident field with coherently scattered field when $\psi_m(t) = (2n+1)\pi$, $n = 0,1,2,\ldots$, while the dark windows appear due to destructive interference when $\psi_m(t) = 2n\pi$, if $S_m(t)$ is negative. The probability has maxima, corresponding to pulses $[1 - S_m(t)]^2\exp(-2\gamma t)$ and minima $[1 + S_m(t)]^2\exp(-2\gamma t)$, relevant to the radiation drop. The most pronounced pulses appear if the intensity of the resonant component $[\sim J_m^2(p)]$ has global extremum. In this case, the maximum intensity of the pulses, predicted by Eq. (5) without exponential factor $\exp(-2\gamma t)$ and assuming that $J_0(2\sqrt{bt}) \approx 0$, which means that the scattered field had time to fully develop, exceeds almost two times the intensity of the radiation field if it would not interact with the absorber. The radiation intensity between bunches is quite small because of the destructive interference, and it is almost an order of magnitude smaller with respect to the pulse maxima.

Qualitatively, the appearance of bunches can be understood from the time evolution analysis of the phase difference of the scattered field and the comb, which is $\psi_m(t) + \pi$ if $S_m(t) < 0$. Time dependence of phase $\psi_m(t)$ is shown in Fig. 2 for $m = 1$ (a), $m = 2$ (b), and $m = 3$ (c) if $\varphi = 0$ and modulation index p has optimal value for each m. The phase $\psi_m(t)$ evolves almost linearly as $(m+p)\Omega t + C$ during the pulse (pulses) formation around $t_p = (n+1/2)T_{\rm vib} = (n+1/2)2\pi/\Omega$ (C is constant within each time interval), and the phase evolution almost stops around $t_s = nT_{\rm vib} = 2\pi n/\Omega$. Durations of linear time evolution and the phase stopping intervals are nearly equal each other and they are nearly confined within the time intervals $(t_p - T_{\rm vib}/4, t_p + T_{\rm vib}/4)$ and $(t_s - T_{\rm vib}/4, t_s + T_{\rm vib}/4)$, respectively. The phase "stops" could be explained by "destructive interference" of two terms in expression for the phase $\psi_m(t)$ at the optimal values of the modulation indexes since at the stops the phase evolution is approximated as $(m-p)\Omega t + C$. Actually, these "phase-stopping" periods are the periods when time evolution of $\psi_m(t)$ changes the slope from $(m+p)\Omega t$ to $(m-p)\Omega t$. Since for the optimal values of the modulation index p we have $p > m$ and approximately the relation $p \approx m+1$ is valid, then the slope of the phase change during formation of pulses is $(2m+1)\Omega t$ and this slope is negative, $-\Omega t$, during the dark windows.

It is interesting to note that tuning into resonance with the $m = -1$ component (if $\varphi = 0$) shifts the position of the pulses with respect to the case of $m = +1$ such that maxima become minima and vice versa. Such a difference is explained by the

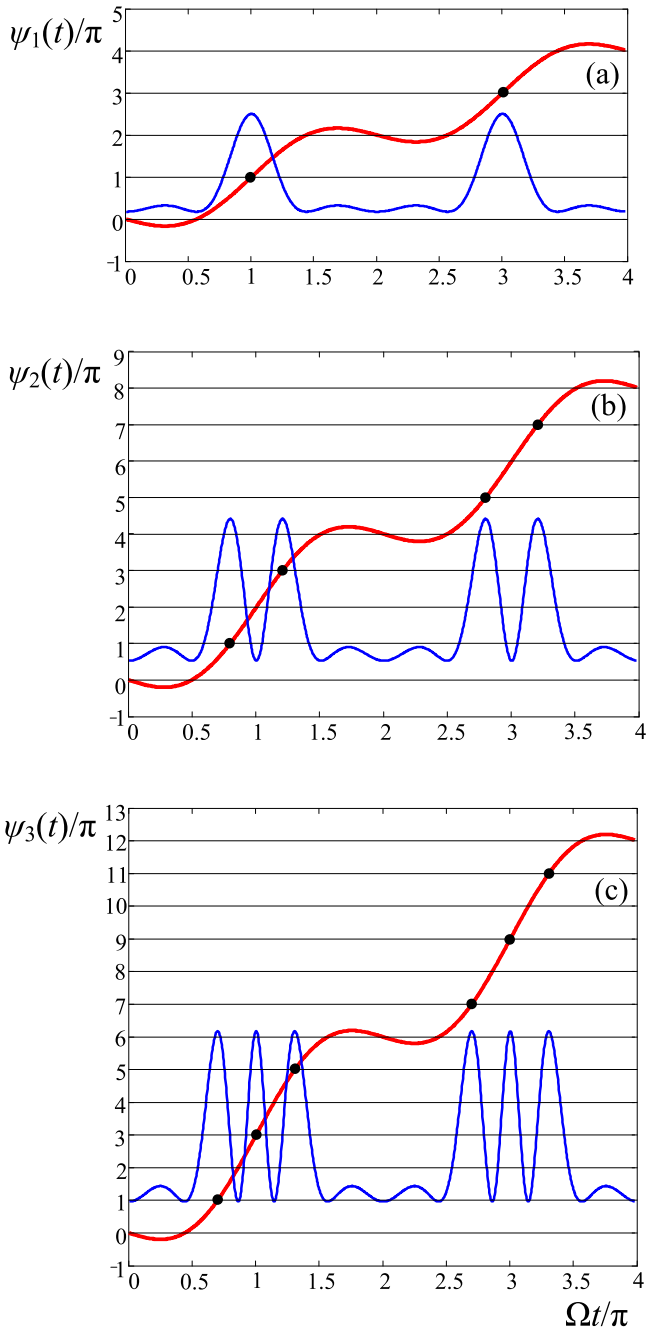

FIG. 2. (Color online) Time evolution of the phase difference of the comb and resonantly scattered field component $\psi_m(t)$ for $m = 1$ (a), $m = 2$ (b), and $m = 3$ (c), thick line in red. Black circles indicate the points when $\psi_m(t) = (2n + 1)\pi$. The values of the modulation index are taken the same as in Fig. 1. The modulation phase is $\varphi = 0$. Thin solid line in blue shows the formation of pulses according to Eq. (5). For visualization, the exponential factor is removed and time-dependent Bessel function is set equal to zero. The amplitudes of the pulses are scaled to fit a half of each plate.

fact that the amplitude of the $m = -1$ component of the comb is proportional to $J_{-1}(p) = -J_1(p)$ and hence the amplitude of the antiphase scattered field [proportional to $S_{-1}(t)$] becomes positive. The details how to move the radiation field from one time bin to the other time bin by changing the phase φ and how this effect can be used to create time-bin qubits and qudits are described in Sec. IV.

III. EXPERIMENT

Our experimental setup was previously used for detecting of slowing down of γ photon in the absorbers with a doublet structure in the spectrum [45], observation of γ echo for γ photon far detuned from resonance with a single-line absorber [35], and for observation of subradiant state transformation to superradiant state in sandwich absorbers by fast displacement of their appropriate layers [37,46]. Recently, we developed a scheme of photon counts selection, inspired by the method [26], and reported our first observation of photon shaping into a train of short pulses [14]. This transformation is performed by tuning the radiation source in resonance with the first sideband $m = 1$.

The experimental setup is based on an ordinary delayed coincidence scheme usually used in measurements of the lifetimes of nuclear states. The schematic arrangement of the source, absorber attached to a piezopolymer transducer, detectors D1 and D2, and electronics is shown in Fig. 3.

As the photon source we use ^{57}Co nuclei in Rh matrix, which decay via a two-photon cascade. The source nucleus decays by electron capture to ^{57m}Fe with nuclear spin $I = \frac{5}{2}$, which decays in turn by emission of a 122-keV photon followed by a 14.4-keV photon (competing with internal conversion) to the ground state with nuclear spin $I = \frac{1}{2}$. The source is mounted on the holder of the Mössbauer drive causing Doppler shift of the 14.4-keV radiation field to tune the source in resonance with the preselected component of the absorber spectrum.

The 122-keV photons are detected by a NaI(Tl) scintillator 25 mm in diameter and 15 mm in length (detector D1), coupled to the RCA 8575 photomultiplier. The lower-energy radiation 14.4 keV is filtered out by a 0.1-mm copper foil placed in front of the 122-keV detector. The output from the

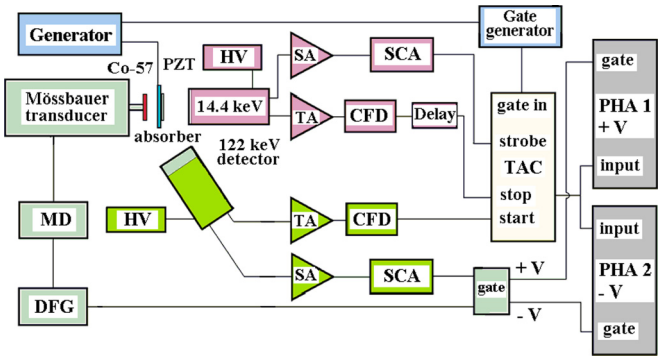

FIG. 3. (Color online) Schematic layout of the experimental setup. TAC is a time to amplitude converter. PHA is a pulse-height analyzer. TA and SA are timing and spectroscopy amplifiers, respectively. SCA is a single-channel analyzer. CFD is a constant fraction discriminator. DFG-MD is the Mössbauer driving unit and function generator. HV is a high-voltage supply. The PVDF transducer (PZT), where the absorber is mounted, is driven by a RF generator, which provides also synchronizing pulses for the Gate generator, gating the START input of TAC.

fast dynode of the photomultiplier is amplified with a timing filter amplifier (2111, Canberra) and triggered by a constant fraction discriminator (2121, Canberra). This timing pulse was employed to produce a start signal for the time-to-amplitude converter TAC/SCA (2145, Canberra). A second detector D2 with a NaI(Tl) scintillator, 25 mm in diameter and 0.1 mm thick, serves as a detector for the 14.4-keV photons. The fast pulse is amplified by the Model 2111 timing filter amplifier and triggered by the Model 2121 constant fraction discriminator to derive a time-pickoff signal, and then it is fed through an adjustable delay line into the stop input of the TAC. The slow pulses from the 14.4-keV detector are amplified with the spectroscopy amplifier SA. The timing single-channel analyzer AMP&TSCA, model 290A, Ortec is utilized to select the 14.4-keV photons. These signals are used as strobe signals to generate the TAC output pulses corresponding to the time intervals between the 122-keV and successive 14.4-keV γ quanta.

As the resonant absorber, we used 25-μm-thick stainless-steel foil (from Alfa Aesar) with a natural abundance ($\sim$2.2% of ^{57}Fe). Optical depth of the absorber is $T_a = 5.18$. The stainless-steel foil is glued on the polyvinylidene fluoride piezotransducer (Measurement Specialties, Inc.), which transforms the sinusoidal signal from the radio-frequency (RF) generator into the uniform vibration of absorber nuclei. RF generator provides also synchronizing pulses for the Gate generator (Ortec Gate&Delay Generator, Model 416A), which gates the START input of TAC. So, the output of the TAC consists of pulses of various heights corresponding to different time intervals between the 122- and 14.4-keV gamma quanta. These pulses are analyzed by two CMCA-550 data acquisition cards (Wissel) in pulse-height mode PHA. The selection of the card to store the signal is gated by the incoming signal from the Mössbauer driver function generator, which defines the frequency of the radiation of the source. When the source is driven with a velocity corresponding to the central frequency or to the mth sideband of the vibrating absorber, the time-domain spectrum is stored in the memory of the first card. The second acquisition card is used to store the time spectrum when the frequency of the radiation of the source is far away from these frequencies. It should be noted that the Gate generator pulses allow TAC and PHA to measure the time-domain spectrum only within a short interval at times, matching the chosen phase of the sinusoidal signal from the RF generator.

Thus, D1 (shielded by copper foil) detects only heralding 122-keV photons and starts the clock. Detection of 14.4-keV photon by D2 stops the clock. In this time-delayed coincidence count technique we reconstruct the time evolution of the photon wave packet transmitted through the resonant absorber. Since time t_0 of the formation of 14.4-keV state nucleus in the source is random, we select only those counts of the heralding 122-keV photons, which are detected within short-time interval Δt around the time t_{ph} satisfying the relation $\Omega t_{ph} = \varphi + 2\pi n$, where n is integer. This selection ensures that the phase of the absorber vibration is always the same for all detected photons. Since small time window of count selection Δt is not zero, we have to average the theoretical expressions for the signal $P(t)$ over small jitter $\Delta\varphi$ of phase φ caused by finite value of Δt.

In Ref. [14], we modulated the absorber with frequency $\Omega = 10.2$ MHz and tuned the radiation field into resonance

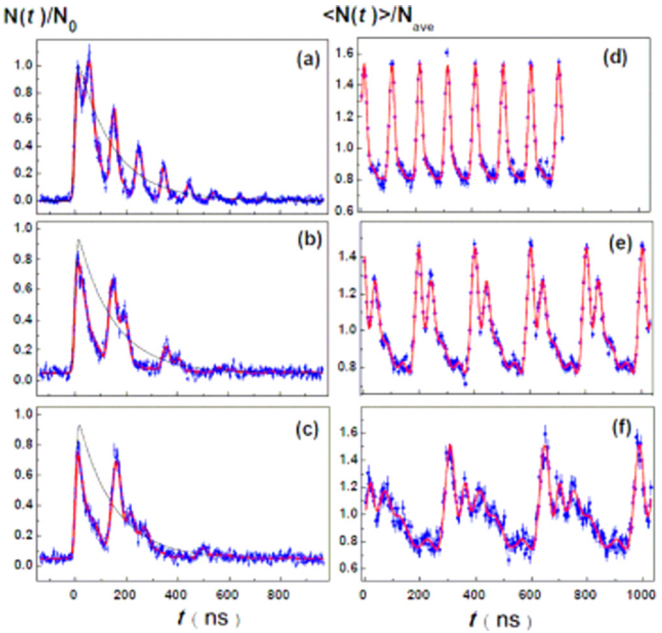

FIG. 4. (Color online) Time dependence of the photon counts $N(t)$ (a)–(c) and the t_0 averaged detection probability of a photon $\langle N(t)\rangle \sim \langle P(t)\rangle_{t_0}$, (d)–(f) at the exit of the absorber vibrating with the frequency 10.2 MHz (a), (d), 4.79 MHz (b), (e), and 2.94 MHz (c), (f). The frequency of the radiation field is tuned into resonance with the first (a), (d), second (b), (e), and third (c), (f) sidebands. Solid line (in red) corresponds to the theoretical fitting, which takes into account the phase jitter for (a)–(c). The experimental results in (d)–(f) are fitted to the exact calculation of the integral in Eq. (7) (solid line in red). $N_{\rm ave}$ is the averaged count rate. The phase, and the phase jitter $\Delta\varphi$ in (a)–(c) are $\varphi = 0$, and $\Delta\varphi = \pi/2$ (a), $\varphi = 0$, and $\Delta\varphi = \pi/3$ (b), $\varphi = -\pi/10$, and $\Delta\varphi = \pi/5$ (c). The modulation index is $p = 1.8$ (a), (d), $p = 3.08$ (b), (e), and $p = 4.21$ (c), (f). The dots with error bars (in blue) show experimental points. Thin line (in black) in (a)–(c) shows the probability time dependence without absorber.

with the first satellite. We observed pulses as short as 28 ns, which are artificially broadened due to $\Delta\varphi \neq 0$ and finite-time resolution of the electronics in our setup limited to 8 ns. To be able to resolve the content of the pulse bunches, for example, consisting of two or three pulses, we had to reduce Ω two or three times, respectively, compared to the modulation frequency, used in our first experiment. The experimental results of the detecting of pulse bunching are presented in Figs. 4(a)–4(c), where time dependence of the number of counts $N(t)$, normalized to the value N_0 without resonant absorbtion, is shown. The contribution of photons emitted with recoil is subtracted. The ratio $N(t)/N_0$ is proportional to the probability $P(t)$. The details of fitting procedure are described in Ref. [14].

To avoid smearing out of the pulses within the bunch due to $\Delta\varphi \neq 0$ we performed experiments without detector D1. Time t_0 is still random but we count time delay of 14.4-keV photon detection with respect to the fixed moments of time $t_{\rm start}$, when the modulation phase φ is the same (differing only by $2\pi n$). In this way, we escape an artificial phase jitter $\Delta\varphi$ inherent to the first scheme of the experiment. What we measure in the

modified scheme is the probability $P(t)$, integrated over time t_0, which varies from $-\infty$ to t, i.e.,

$$\langle P(t)\rangle_{t_0} = 2\gamma_s \int_{-\infty}^{t} P(t-t_0)dt_0. \tag{7}$$

Calculation of this integral for the analytical approximation (5) gives

$$\langle P(t)\rangle_{t_0} = 1 - 2V_m(p)\cos\psi_m(t) + U_m(p), \tag{8}$$

where $V_m(p) = J_m(p)[1-\exp(-T_a/4)]$, $U_m(p) = V_m^2(p) + J_m^2(p)\exp(-T_a/2)[I_0(T_a/2)-1]$, and $I_0(T_a/2)$ is the modified Bessel function of zero order. We notice that for a single-line absorber (not vibrating), a steady-state transmission of resonant γ quanta is proportional to the function $\exp(-T_a/2)I_0(T_a/2)$, where T_a is the optical depth of the absorber. The exact expression for $\langle P(t)\rangle_{t_0}$, obtained without analytical approximation (5), looks very complicated and does not allow simple interpretation and analytical analysis (see Ref. [33]). Meanwhile, our approximation slightly deviates from this exact result. However, if the contribution of two neighboring sidebands, blue and red detuned from resonant component, are taken into account, then the difference becomes negligible (see Appendix B). Figures 4(d)–4(f) demonstrate the results of our time-delayed measurements with respect to a fixed phase of the vibrations. In spite of poor time resolution of our electronics the pulses within bunches are clearly seen.

IV. TIME-BIN QUBITS VIA PULSE BUNCHING

Single photons are ideal information carriers for quantum communication and computing. In many quantum protocols, photon polarization is used as the information carrier [20]. Time-bin qubits, proposed and implemented in Refs. [22,23], were early examples of how the time domain can be involved in the information coding by splitting a single photon into two pulses with a fixed phase difference and controllable amplitudes. The information carried by such a photon is well protected during its propagation in optical fiber since cross talk, usually influencing polarization states of a photon, is excluded. Time coding of information is implemented in [22,23] by an interferometer having different arm lengths and a phase shifter placed in the long arm. Unbalanced three path interferometers were used in [24] to create three-state quantum objects (qutrits). Interferometers are practical to split short single-photon pulses produced by parametric down conversion and lasting hundreds of picoseconds or shorter. Therefore, one can use the difference of the interferometer arm lengths as small as several centimeters or shorter to split a photon in time into distinguishable pulses. Recently, creation of time-bin qubits, qutrits, and ququads with long coherence length photons has been performed by pumping a single atom in a QED cavity having relatively small size [25].

Time-bin qubits, produced by transmitting a single photon through unbalanced interferometers, have analogy with spin $\frac{1}{2}$ since the output photon can be expressed as a coherent superposition of two states $|\text{short}\rangle$ and $|\text{long}\rangle$ [22]:

$$|a\rangle_{TB} = \alpha|\text{short}\rangle + \beta|\text{long}\rangle, \tag{9}$$

where $|\text{short}\rangle$ and $|\text{long}\rangle$ describe photon parts propagating through the short and long arms of the interferometer, respectively. The relative norm and phase of the coefficients are determined by the coupling ratio of the beam splitter, which splits a photon into the arms of the interferometer, and the phase shifter, placed in the long arm. By varying the coefficients α and β, one can span the two-dimensional Hilbert space by the state (9). Hence, this state is equivalent to the state of spin $\frac{1}{2}$ covering two-dimensional Poincare sphere. Ideally, the state (9) can be created without losses.

Photon shaping, proposed in [26], also produces a photon consisting of time bins. However, this shaping is performed by transmitting a photon through the electro-optic amplitude modulator, which consists of phase modulators in both arms of a Mach-Zehnder (MZ) interferometer. One port of the output beam splitter of the MZ interferometer is terminated so that the portion of the photon wave function that is not transmitted is lost. One can roughly estimate the fundamental losses of the amplitude modulation scheme as follows. If, during the production of the time-bin qubit, half of the photon probability is lost (since it is not transmitted but "converted" into the dark windows at the output port), then the losses are simply 50%.

Similar losses are also inherent to the shaping of ultrashort pulses produced by acousto-optic modulators (AOM) [47]. For example, coding the information into the spectrum of the pulse by its Bragg scattering on the acoustic wave, generated by RF pulses in AOM [48], also selects and cuts only a part of the input pulse energy. As a result, the smooth broadband spectrum of the radiation pulse becomes comblike since some parts of it are not scattered in the Bragg direction. In this method of the pulse shaping the acoustic wave propagates very slowly with respect to the pulse duration and the pulse sees the wave as a standstill structure whose oscillation period is extremely large with respect to the pulse duration. In contrast, we demonstrate the pulse shaping by the absorber vibrating with the period, which is much shorter than the pulse duration.

Here, we propose two algorithms as to how pulse bunching can be used to create and operate with time-bin qubits. Assume that the phase of absorber vibrations is zero, $\varphi = 0$, and we tune the radiation source in resonance with the first satellite $\omega_s = \omega_a + \Omega$. Then, the pulses are formed at the moments of time $t_p = (2n+1)T_{\text{vib}}/2$, where $n = 0,1,2,\ldots$. The dark windows are formed around the moments of time $t_d = nT_{\text{vib}}$. The illustration of these pulses and dark windows is given in Fig. 5(a). In the bottom panel [Fig. 5(d)], the evolution of the radiation phase $\sin(\Omega t)$ is shown. It is divided into bins A and B. The A bins are centered at times t_p where the pulses are formed due to constructive interference of the incident and coherently scattered radiation fields. The B bins are centered at times t_d where dark windows appear due to destructive interference of the incident and coherently scattered radiation fields. The length of these bins is equal to half a period of the vibrations $T_{\text{vib}}/2$.

Following, we assume that we have a local oscillator, for example, a generator producing the voltage oscillating according to the function $\sin(\Omega t + \varphi_{lo})$ with phase $\varphi_{lo} = 0$. The same oscillator generates mechanical vibrations of the absorber with tunable phase φ. If $\varphi = 0$, all the pulses are formed at the output of the absorber in A bins and dark windows are located in B bins [see Fig. 5(a)]. If $\varphi = \pi$, the

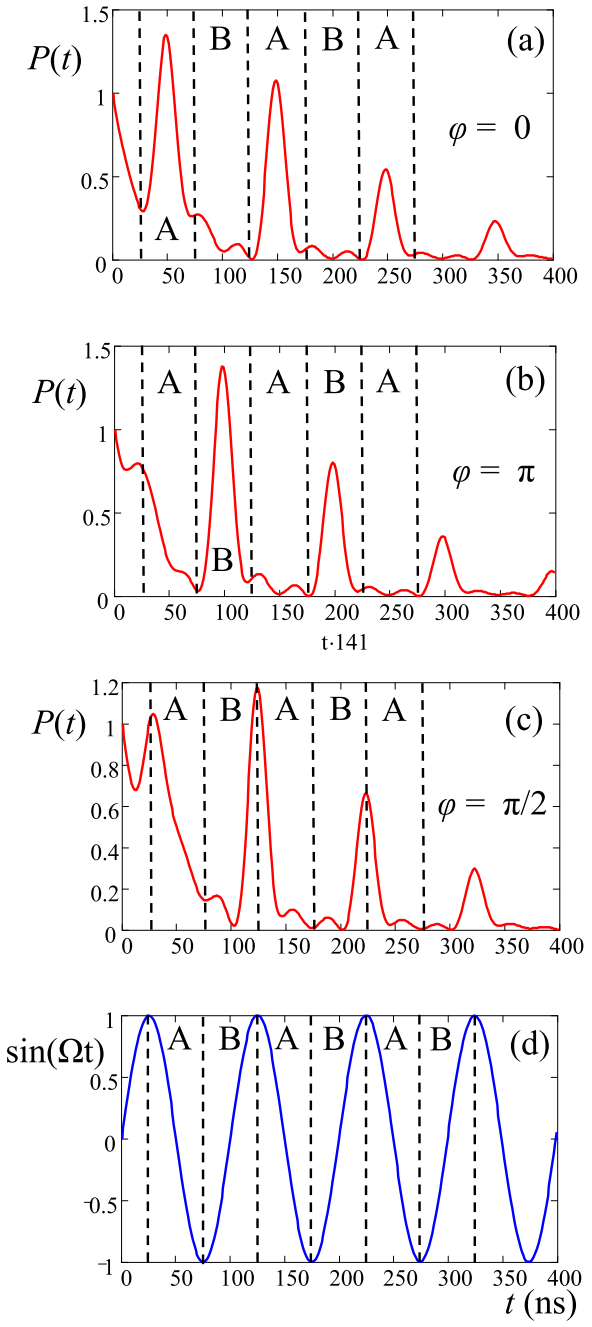

FIG. 5. (Color online) (a)—(c) Time dependence of the detection probability of a photon, which is in resonance with the first satellite of the central component of the frequency comb $\omega_s = \omega_a + \Omega$. The vibration frequency of the absorber is $\Omega = 10$ MHz and the modulation index is $p = 1.8$. Effective thickness of the absorber is $T = 12$. The value of the vibration phase φ is indicated in each plot. (d) The phase evolution of the radiation field interacting with the vibrating absorber in its reference frame if $\varphi = 0$. The value of the field phase is normalized to the modulation index p. Dashed vertical lines separate time bins A and B (see the text for details).

pulses are generated in B bins, while dark windows are located in A bins [see Fig. 5(b)]. If $\varphi = \pi/2$, then the radiation field is equally distributed among A and B bins [see Fig. 6(c)]. Thus,

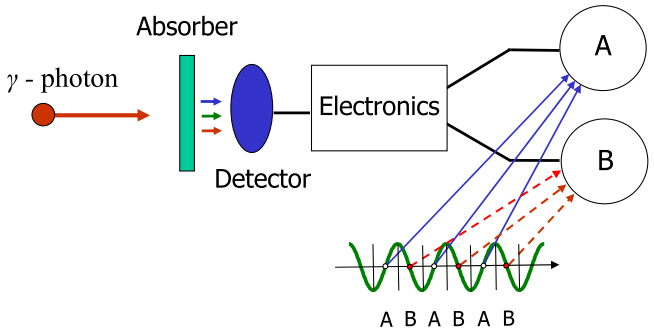

FIG. 6. (Color online) Schematic presentation of the method as to how with one detector (dark oval in blue) the pulses, formed by the vibrating absorber from the single γ photon, can be transferred by electronics (data acquisition system) into bins A and B. The correspondence of these bins to the time evolution of the oscillating phase (waving line in green) is shown in the bottom.

we are able to construct a photon state

$$|a\rangle_{PB} = |\cos(\varphi/2)||\mathrm{A}\rangle + |\sin(\varphi/2)||\mathrm{B}\rangle, \tag{10}$$

by appropriate change of the vibration phase φ.

In optical domain, such bins can be spatially separated by a router based, for example, on the Mach-Zehnder interferometer with a phase shifter placed in one of the interferometer arms. If this phase shifter is fed by the local oscillator, one can send the radiation field from bins A to the detector A and from bins B to the detector B in accordance with the phase evolution shown in Fig. 5(d). If the phase modulator of the radiation field, placed between the source and absorber to create a frequency comb, has the modulation phase φ, which is the same as $\varphi_{lo} = 0$, then only the detector A will detect the radiation field. If this phase has a π shift with respect to $\varphi_{lo} = 0$, only the detector B will detect the radiation field. If the modulation phase is $\pi/2$, both detectors have the same probability of photon detection. In such a way, a time-bin qubit (10) can be produced.

The pulses (bins) $|\mathrm{A}\rangle$ and $|\mathrm{B}\rangle$ are always in phase with the incident radiation field (see Discussion section for details). Since there is no variable phase difference between the components of state (10), this state does not cover the whole Poincare sphere. If we place phase shifters in the paths of the time bins A and B after the router, then state (10) can be modified as

$$|a\rangle_{1/2} = \cos(\varphi/2)|\mathrm{A}\rangle + e^{i\phi}\sin(\varphi/2)|\mathrm{B}\rangle, \tag{11}$$

where ϕ is a phase difference, which is introduced by the phase shifters between paths traveled by the bins A and B. We notice that here, as it is usual in quantum mechanics, the phase of state $|a\rangle_{1/2}$ as a whole is not defined since it may be arbitrary. Now, state (11) can be considered as state, which is equivalent to spin $\frac{1}{2}$.

In the γ domain, the routers are not currently available. However, the main elements, from which they could be constructed, have been recently developed. They are high-efficient back-reflecting mirrors [8], efficient beam splitters [12], and tight focusing facilities [11]. Meanwhile, even without routers we can distinguish A and B bins electronically (see Fig. 6). In time-delayed coincidence counting technique we have only

two detectors. One is for the heralding 122-keV photon, which starts the clock, and the other is for the resonant 14.4-keV photon, which stops the clock. We distinguish detection events of the 14.4-keV photon in time by multichannel data acquisition system with quite short duration of each channel (see, for example, Refs. [35,45]). This scheme can be easily modified to simulate effective detectors A and B electronically, having physically only one detector for the resonant γ photon.

We assume that in the optical domain it is possible to produce qubits of higher dimension, known as qudits, by transformation of a single photon into bunches of pulses and by routers. We estimate that it would be hard to vibrate the absorber piston like with large amplitude comparable with the wavelength of the optical radiation field. The simplest way to produce the phase modulation of the radiation field with high frequency and large deviations is to use the phase modulators. If the modulation index is large enough, the single frequency radiation field is transformed into a frequency comb with desirable properties. As an example, we consider the case when the second satellite of the central component of the radiation field incident to the absorber is tuned in resonance $\omega_s = \omega_a + 2\Omega$ and modulation index has optimal value $p = 3.1$, i.e., it is close to π. Then, the single-photon wave packet after passing through the absorber is split into bunches of pulses with two pulses in each bunch [see Fig. 7(a), solid curve in red]. Now, time can be grained into time bins A, B, C, and D with a duration $T_{\rm vib}/4$ each. If the phase of the phase modulation (PM) is zero $\varphi = 0$, i.e., it coincides with the phase of the local oscillator φ_{lo}, then only bins A and B contain the radiation pulses, while bins C and D fall into dark windows [see Fig. 7(a), solid curve in red]. If the phase of PM is $\varphi = -\pi/2$, the pulse bunches are shifted to a quarter of modulation period and then bins B and C are occupied while bins A and D are almost empty [see Fig. 7(a), dotted line in blue]. Changing the modulation phase further ($\varphi = -\pi$) we can move pulses from bins B and C to bins C and D [see Fig. 7(b), dotted line in blue]. If the modulation phase is $\varphi = -3\pi/2$, the pulses occupy D and A bins only [see Fig. 7(c), dotted line in blue].

To separate spatially time bins A, B, C, and D we propose to transmit the radiation field through a set of routers R1, R2, and R3 (see Fig. 8). Router 1 (R1) separates the couple of time bins A and B from a couple of time bins C and D. R1 is synchronized with the local oscillator such that the first half a period $T_{lo} = T_{\rm vib}$ of the local oscillator the radiation field is sent to the router R2 and the second half of the oscillation period the radiation field is sent to the Router 3. These routers, R2 and R3, switch the path of the radiation field two times faster than R1 but with the same phase φ_{lo}. Then, the radiation field, contained in time bin A, will always go to the detector A. The same is realized for time bins B, C, and D. The radiation field contained in these time bins will go to the detectors B, C, and D, respectively (see Fig. 8). By changing the phase of PM φ, with respect to the phase of local oscillator φ_{lo}, one can control the population of bins A, B, C, and D.

It is already mentioned that single pulses, generated when we tune in resonance the first satellite (see Fig. 5), are in phase with the incident radiation field. When we tune in resonance the second satellite, two pulses are grouped in a bunch (see Fig. 7). The first pulse in a bunch has a phase shift $\pi/2$ with

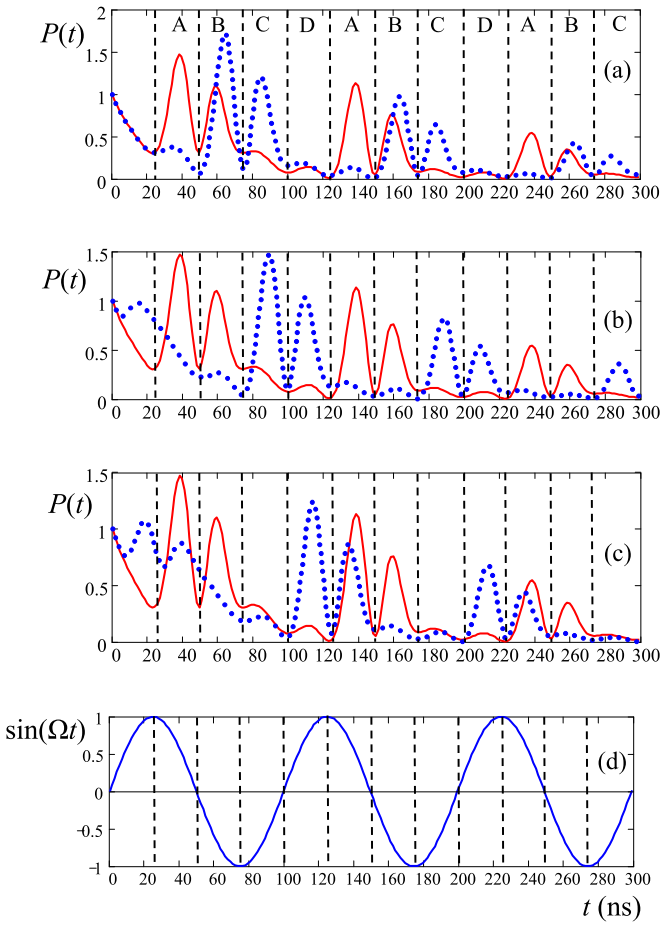

FIG. 7. (Color online) (a)–(c) Time dependence of the detection probability of a photon with comb spectrum, whose second satellite of the central component is in resonance with the absorber $\omega_s = \omega_a + 2\Omega$. Frequency of the phase modulation is $\Omega = 10$ MHz and the modulation index is $p = 3.1$. Effective thickness of the absorber is $T = 12$. The value of the modulation phase φ is zero for solid line (in red) and it is $-\pi/2$ (a), $-\pi$ (b), and $-3\pi/2$ (c) for dotted lines (in blue). (d) The phase evolution of the field after the phase modulator (normalized to the modulation index p) if $\varphi = \varphi_{lo} = 0$. Dashed vertical lines separate time bins A, B, C, and D (see the text for details).

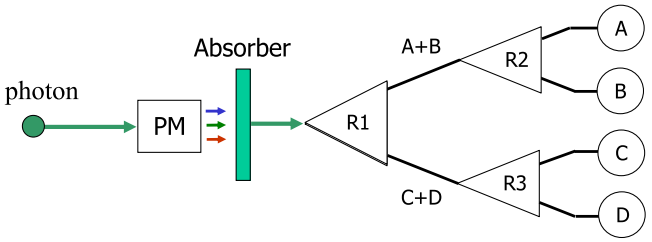

FIG. 8. (Color online) Spatial separation of pulses from bunches. Single-photon radiation field is transformed to the frequency comb by phase modulator PM. Passing through the absorber the single-photon wave packet is shaped into pulses, which are spatially separated by routers R1, R2, and R3 such that bins A, B, C, and D are sent to the corresponding detectors A, B, C, and D (see the text for details).

respect to the incident field and the second pulse has opposite phase $-\pi/2$. This feature could be used to implement some operations with bins A, B, C, and D if we make them interfere after passing appropriate bins through a delay line.

Our scheme of photon transformation into bunches of pulses is not ideal since the vibrated absorber introduces losses. However, they are small. We estimate roughly the integrated absorbtion as follows. If the m component of the comb is in resonance with the absorber, then time-integrated intensity of the transmitted radiation

$$\langle P(t)\rangle_t = 2\gamma_s \int_{-\infty}^{+\infty} P(t)dt \tag{12}$$

can be approximated as

$$\langle P(t)\rangle_t = 1 - J_m^2(p)[1 - e^{-T_a/2} I_0(T_a/2)]. \tag{13}$$

The first term (unity) in the right-hand side of the equation is just the intensity of the frequency comb. The second term $J_m^2(p)$ is the intensity of the resonant component whose transmission through the absorber gives the third term $J_m^2(p)\exp(-T_a/2)I_0(T_a/2)$. If $m = 1$, we lose 25% of photon probability when generating the train of single pulses. If $m = 2$, we lose 17% of photon probability when generating two pulse bunches. If $m = 3$, we lose 14% of photon probability when generating three pulse bunches. These estimates are done for the absorber with optical thickness $T_a = 5.2$ and optimal values of the modulation index p for each m. Decrease of losses with increase of number of pulses in a bunch is due to the decrease of the first maximum of $J_m^2(p)$ with increase of m. The losses in our method are appreciably smaller than in the scheme of photon shaping, based on electro-optic amplitude modulator [26].

There is another option to shape a photon into time bins with the help of a sandwich absorber. Let us consider the case when the source is vibrated with the frequency Ω and the probability amplitude of the emitted photon is described as

$$a_s(t) = a_L(t)\exp[i\Psi(t)], \tag{14}$$

where $a_L(t)$ is defined in Eq. (2), $t_0 = 0$, and $\Psi(t) = p\sin(\Omega t + \varphi)$. We propose to use a sandwich absorber, which consists of two samples. One is tuned by Mössbauer drive in resonance with the first sideband $\omega_s + \Omega$ of the frequency comb [Eq. (14)] and another one is tuned in resonance with -1 sideband $\omega_s - \Omega$ by its own separate Mössbauer drive. We propose to use the absorbers of the wedge form as shown in the inset into Fig. 9. Moving the wedges up or down such that their total thickness remains the same, one can change their individual thicknesses for the radiation field propagating in the transverse direction shown by the arrow (in red). The radiation field is collimated by a diaphragm such that only a small spot on the absorber is irradiated. Therefore, thickness of the sandwich absorber is almost uniform in the radiation beam area. The probability amplitude of the radiation field at the output of the first sample of the sandwich absorber is

$$a_{s1}(t) = a_s(t) - b_1 \int_0^t a_s(t-\tau,l) j_1(b_1\tau) e^{-\gamma_{a1}\tau - i\omega_{a1}\tau} d\tau, \tag{15}$$

where $b_1 = \gamma_{a1}T_{a1}/2$, γ_{a1} is the decay rate of the nuclear coherence in the first sample, $T_{a1} = \alpha_B l_1$ and l_1 are effective and physical thickness of the first sample, respectively, ω_{a1}

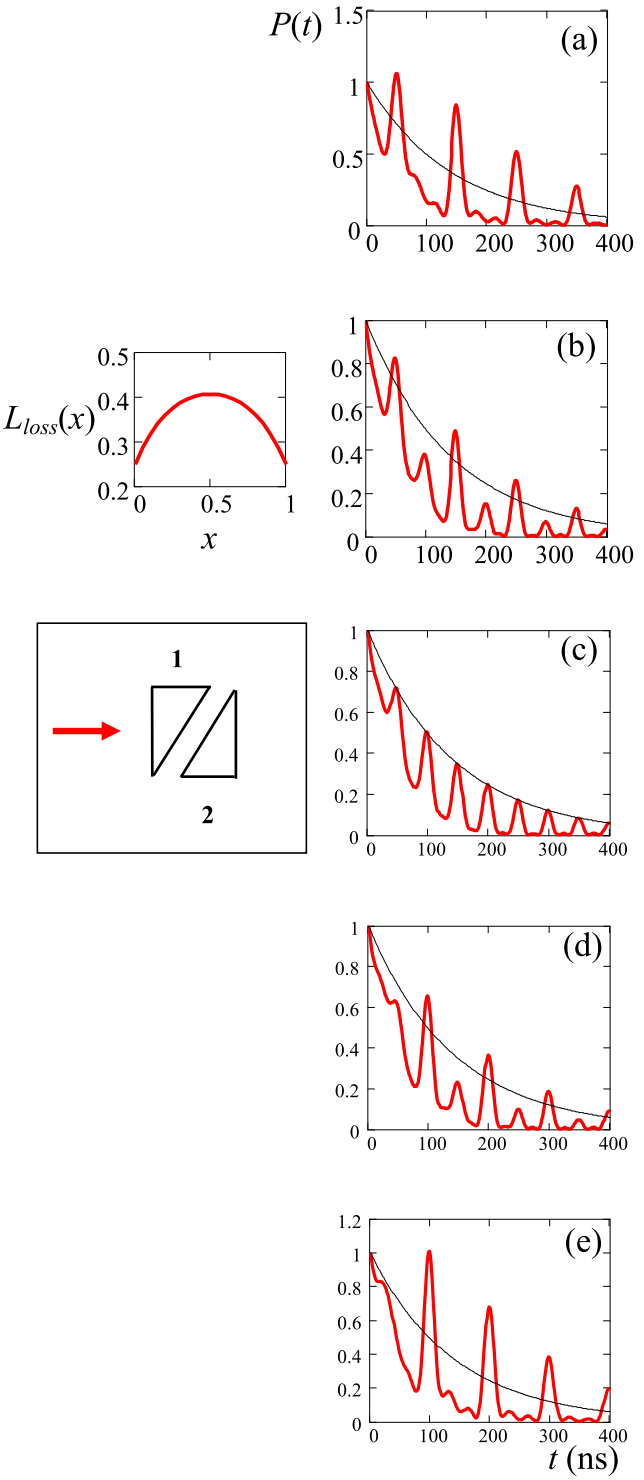

FIG. 9. (Color online) Time evolution of the detection probability of a photon $P(t)$ at the output of the sandwich absorber. The effective thickness of the absorbers are $T_{a1} = T_{\rm tot}$ and $T_{a2} = 0$ in (a), $T_{a1} = 2T_{\rm tot}/3$ and $T_{a2} = T_{\rm tot}/3$ in (b), $T_{a1} = T_{a2} = T_{\rm tot}/2$ in (c), $T_{a1} = T_{\rm tot}/3$ and $T_{a2} = 2T_{\rm tot}/3$ in (d), and $T_{a1} = 0$ and $T_{a2} = T_{\rm tot}$ in (e), where $T_{\rm tot} = 5.2$ is the total thickness of the absorber. The schematic arrangement of the sandwich absorber (consisting of the wedges 1 and 2) and the propagation direction of the radiation field are shown in the inset. The plot in the inset shows dependence of losses $L_{\rm loss}(x)$ on the ratio of thicknesses of the sandwich elements $x = T_{a2}/T_{\rm tot}$.

is the resonant frequency of the first sample tuned by its Mössbauer drive. The probability amplitude of the radiation field at the output of the second sample of the sandwich absorber is

$$a_{s2}(t) = a_{s1}(t) - b_2 \int_0^t a_{s1}(t-\tau,l) j_1(b_2\tau) e^{-\gamma_{a2}\tau - i\omega_{a2}\tau} d\tau, \tag{16}$$

where $b_2 = \gamma_{a2} T_{a2}/2$, γ_{a2} is the decay rate of the nuclear coherence in the second sample, $T_{a2} = \alpha_B l_2$ and l_2 are effective and physical thickness of the second sample, respectively, ω_{a2} is the resonant frequency of the second sample tuned by its Mössbauer drive. If $\gamma_{a1} = \gamma_{a1} = \gamma$, where γ is the decay rate of the radiation field, emitted by the source, and both samples are tuned in resonance with spectral components, as discussed above, i.e., $\omega_{a1} = \omega_s + \Omega$ and $\omega_{a2} = \omega_s - \Omega$, then Eq. (16) can be approximated as

$$a_{s2}(t) = a_s(t) - J_1(p) a_L(t)[2i \sin(\Omega t) - e^{i\Omega t} J_0(2\sqrt{b_1 t}) + e^{-i\Omega t} J_0(2\sqrt{b_2 t})], \tag{17}$$

where $\varphi = 0$ for simplicity. Time evolution of the probability $P(t) = |a_{s2}(t)|$ for different values of b_1 and b_2 if $b_1 + b_2 = b$ (b is constant) is shown in Fig. 9. The vibration frequency of the source is $\Omega = 10$ MHz and the decay rate of the nuclear coherence of the source and the elements of the sandwich absorber is $\gamma = 1.1$ MHz. It is clearly seen that the distribution of the amplitudes of the pulses in the time bins can be regulated by moving sandwich up or down. Such a movement changes individual thickness of the absorbers.

We estimate radiation losses in the second scheme in a similar way as it is done in the first scheme. Time-integrated intensity of the radiation, transmitted through the sandwich, is

$$\langle P_s(t)\rangle_t = 1 - J_1^2(p)[2 - e^{-T_{a1}/2} I_0(T_{a1}/2) - e^{-T_{a2}/2} I_0(T_{a2}/2)], \tag{18}$$

where T_{a1} and T_{a2} are optical thicknesses of the elements of the sandwich. Here, we use the identity $J_{-1}^2(p) = J_1^2(p)$. The meaning of the terms in Eq. (18) is the same as in Eq. (13) since for the sandwich two components of the comb ($m = 1$ and -1) interact separately with their own resonant element of the sandwich. Simple calculations show that if $T_{a1} + T_{a2} = T_{tot} = 5.2$, i.e., the sandwich has the same optical thickness as we take in the first scheme, then the radiation losses are also 25% if $T_{a1} = 5.2$, $T_{a2} = 0$ [see Fig. 9(a)] or $T_{a1} = 0$, $T_{a2} = 5.2$ [see Fig. 9(e)]. When T_{a1} tends to be equal to T_{a2}, then losses increase taking maximum value 40% if $T_{a1} = T_{a2} = T_{tot}/2$ [see Fig. 9(c)]. Their dependence $L_{\rm loss}(x)$ on the relative thickness of the sandwich elements $x = T_{a2}/T_{\rm tot}$ is shown in the inset.

V. DISCUSSION

Mathematically, the interaction of the frequency comb, created by vibrating the source or by another method of the phase modulation of a single-line narrow-bandwidth radiation field, with the narrow linewidth absorber and the interaction of a single-line narrow-bandwidth radiation field with vibrating absorber or absorber whose resonant frequency is modulated can be described similarly. In both cases, we obtain the same expression for the radiation intensity, transmitted through the absorber. However, physically they are different. For example, the amplitude of a single-photon γ-radiation field, transmitted through the vibrated absorber, can be approximated as

$$a_L(t,l) = a_L(t)[1 + S_m(t) e^{im(\Omega t+\varphi) - ip\sin(\Omega t+\varphi)}], \tag{19}$$

if the vibration frequency is large ($\Omega \gg \gamma$) and resonant condition $\omega_s = \omega_a + m\Omega$ is satisfied. This amplitude for the vibrated source and absorber at rest is

$$a_L(t,l) = a_L(t)[e^{ip\sin(\Omega t+\varphi)} + S_m(t) e^{im(\Omega t+\varphi)}]. \tag{20}$$

For the vibrated absorber, the phases of the produced pulses coincide with the phase of the incident single-line radiation field. For the vibrated source, the phases of the pulses are $m(\Omega t + \varphi) - (2n+1)\pi$ since pulses appear when $\psi_m(t) = (2n+1)\pi$, where $\psi_m(t) = m(\Omega t + \varphi) - p\sin(\Omega t + \varphi)$ and n is the pulse number in a sequence (see Fig. 2). For a single pulse in a bunch ($m = 1$), pulses appear when $\Omega t + \varphi = (2n+1)\pi$ and they have the same phase. If $m > 1$, we have m pulses in a bunch, and the phases of pulses in a bunch are different.

Physical processes responsible for the pulse generation are also different in the considered cases. If the source vibrates, we have interference of the resonantly scattered component of the radiation field with the comb. If the absorber vibrates coherently, it induces Raman scattering of the monochromatic radiation field producing frequency comb (see, for example, Ref. [49]). Similar comb is also produced by the source vibration (see, for example, Ref. [50]). We have to emphasize that in the γ domain these comb structures were observed in many experiments [49–60]. However, to the best of our knowledge, no transients were observed for a single γ photon at high frequencies ($\Omega \gg \gamma$), except transients, averaged over time of formation of the 14.4-keV excited state nucleus in the source t_0, i.e., without use of detector D1 (see, for example, Refs. [55,56]). Moreover, no attempts were made earlier to observe pulse bunching, which is reported in this paper and found by tuning in resonance mth sideband of the absorption spectrum and choosing appropriate modulation index p to maximize the intensity of the mth sideband.

In the optical domain, generating of the comb structure, which is produced by coherently induced molecular vibrations, is reported in Ref. [61]. Short and strong nonresonant pulse (30 fs) excites uniform molecular vibrations of gaseous SF_6. Then, long pulse (200 fs) of much smaller intensity propagates through the gas of vibrating molecules. Coherent vibration of the molecules transforms the resonant laser radiation into higher-order Stokes and anti-Stokes components. The measured output Raman spectra are quite reminiscent of the comb structures, observed in the γ domain, especially in the intensity dependence of the comb components on the modulation index, varied in the experiment by changing the gas pressure. However, the physical process of generating sidebands in [61] does not involve any resonant transitions in the molecules and the pulse bunching was not observed.

We would like to mention also two recent interesting proposals of forming the frequency combs, accordingly, in x-ray range (based on imprinting the structure of an optical frequency comb onto the emitted, x-ray resonance fluorescence

spectrum of atoms [62]) and in γ-ray range (based on nonlinear Compton scattering of a broad bandwidth radiation [63]).

VI. CONCLUSION

We suggested a method to shape single-photon wave packets into bunches of m pulses by transmission through the optically thick single-line absorber, which is mechanically vibrated. The pronounced shaping is performed by tuning radiation field into resonance with the mth vibrational sideband, whose intensity is maximized by the proper choice of the vibration amplitude. We found a simple analytical solution clearly explaining formation of bunches of pulses under these conditions. Our method allows to shape long-coherence-length single-photon radiation field with the help of geometrically small devices.

We experimentally demonstrated this method in the γ domain for 14.4-keV photons, emitted by ^{57}Co radioactive source. These photons interact with the resonant absorber, which is a stainless-steel foil. The 14.4-keV photons with 42-m coherence length were shaped into the trains of single, double, and triple pulses using 25-μm-thick foil with a natural abundance of ^{57}Fe. The same result could be achieved using 0.5-μm-thick foil if it would be 100% enriched with ^{57}Fe.

We discussed potential applications of this technique for realization of time-bin qubits in the γ domain. We suggested two different ways to control the relative amplitudes of the time bins in the qudit, i.e., via the variation of the vibration phase, or via the variation of relative optical thicknesses of two absorbers, which are tuned to Stokes and anti-Stokes sidebands of the same order, respectively.

We believe that our method of controlling the shape of a single-photon wave packet is also applicable in the optical domain for atoms, molecules, or impurity ions resonantly interacting with the radiation field. The proposed method could complement the existing arsenal of a single-photon shaping and time-bin qudit preparation techniques. The modulation of the resonant interaction of the field with atoms, molecules, or impurity ions can be realized by time-dependent Zeeman or Stark effects, which are capable to produce extremely short pulses [64,65], by coherent molecular vibrations, which could be induced by a short nonresonant pulse of large intensity, as it is demonstrated in [61], or by phase modulators. The method is capable to make fine tuning the amplitudes, time, and intervals between pulses produced from a single photon.

ACKNOWLEDGMENTS

This work was partially funded by the Russian Foundation for Basic Research (Grants No. 15-02-09039-a, No. 14-32-50091-mol-nr, and No. 14-29-07152), the Program of Competitive Growth of Kazan Federal University funded by the Russian Government, the RAS Presidium Program "Actual problems of low temperature physics," the National Science Foundation (Grant No. PHY-1307346), and the Robert A. Welch Foundation (Award No. A-1261). V.A.A. acknowledges a personal grant for young scientists from Dynasty Foundation. We are grateful to A. Kalachev for the fruitful discussions.

APPENDIX A

If the modulation frequency Ω is much larger than the half-width of the absorption line γ_a and only one spectral component of the frequency comb is tuned in resonance with the absorber, then one can neglect the interaction with other nonresonant components. Such an idealization works quite well if the spectrum of a single-line radiation source has rapidly falling tails as it is inherent, for example, to the Gaussian spectrum. In case of heralded single photons, the spectrum of the radiation field is $a(\omega) = i/(\omega - \omega_s + i\gamma_s)$ (see, for example, Ref. [45]). This spectrum has long tails falling as $\sim 1/(\omega - \omega_s)$. They appear because the front of the photon wave packet has sharply rising leading edge. Therefore, many satellites start wringing immediately after this front comes, however, with small amplitudes. As a result, the approximate Eq. (5) describes the modulation of a single-photon field with small misfit compared with exact Eq. (6). Following, we improve fitting by taking into account the interaction with the nearest satellites of the resonant component.

The propagation of a single-line radiation field with carrier frequency ω_s through a single-line absorber with resonant frequency ω_a is described by Eq. (6). It is derived by the convolution of the incident field amplitude with the response function (Green function) of a single-line absorber, which is

$$R(t) = \delta(t) - \Theta(t)e^{-(i\omega_a+\gamma_a)t}bj_1(bt), \tag{A1}$$

where $\delta(t)$ is the Dirac delta function (see, for example, Refs. [33,45,66]). According to Eq. (6), the coherently scattered field amplitude is

$$a_{\rm sct}(t-t_0,l) = -\Theta(t-t_0)b\int_0^{t-t_0} a_A(t-t_0-\tau,l)j_1(b\tau) \times e^{-\gamma_a\tau - i\omega_a\tau}d\tau. \tag{A2}$$

If the m component of the frequency comb, Eq. (1), is in resonance with the absorber, i.e., $\omega_s = \omega_a + m\Omega$ and $\gamma_s = \gamma_a$, then the amplitude of the coherently scattered field for this component is reduced to

$$a_m(t-t_0,l) = a_L(t-t_0,l)S_m(t-t_0)e^{im(\Omega t+\varphi)}, \tag{A3}$$

where for simplification of the notations we drop the index sct. The contribution of the satellites $\omega_s - (m \pm n)\Omega$, where $n = 1,2,3,\ldots$, was not taken into account in Eq. (5). According to Eq. (A2), the amplitudes of the fields, scattered by the satellites, are

$$a_{m\pm n}(t-t_0,l) = -a_L(t-t_0,l)J_{m\pm n}(p)e^{i(m\pm n)(\Omega t+\varphi)}b \times \int_0^{t-t_0} j_1(b\tau)e^{-(\gamma_a-\gamma_s)\tau \mp in\Omega\tau}d\tau. \tag{A4}$$

Then, the exact result (6) can be expressed as follows:

$$a_{\rm ext}(t,l) = a_A(t,l) + \sum_{n=-\infty}^{+\infty} a_{m+n}(t,l), \tag{A5}$$

where $t_0 = 0$. Comparison of the exact result with the approximation, when only two nearest satellites ($n = \pm 1$) of the resonant component ($n = 0$) are taken into account, is shown in Fig. 10. In this case misfit is almost negligible. To estimate the contribution of the satellites, we calculated the

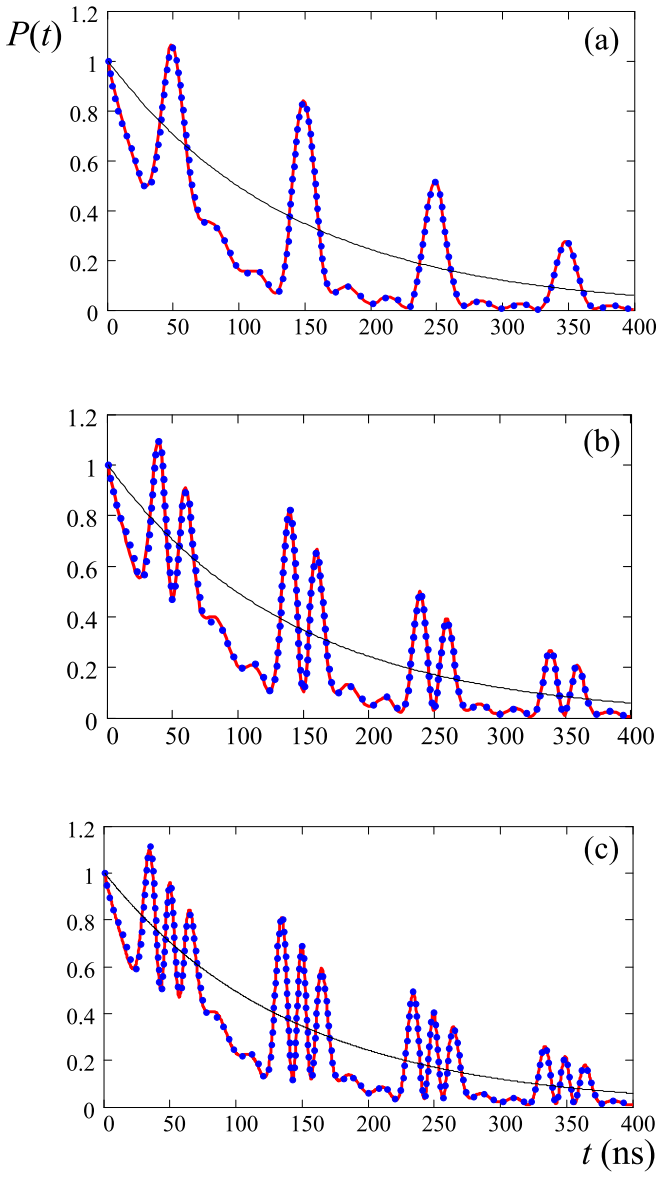

FIG. 10. (Color online) Comparison of the exact result for the probability $P(t)$, derived from Eq. (6) (solid line in red), with that, which is obtained from Eq. (A5), where only the resonant component $n = 0$ and two nearest satellites $n = \pm 1$ are taken into account (dotted line in blue). The parameters and notations are the same as in Figs. 1(a)–1(c).

integral

$$K_{\pm n}(t) = b\int_0^t j_1(b\tau)e^{\pm in\Omega\tau-(\gamma_a-\gamma_s)\tau}d\tau \tag{A6}$$

in Eq. (A4) with the help of the method, presented in Refs. [41,44,67,68]. The result is

$$K_{\pm n}(t) = 1 - e^{-ib/[\pm n\Omega+i(\gamma_a-\gamma_s)]} + M_{\pm n}(t), \tag{A7}$$

$$M_{\pm n}(t) = e^{\pm in\Omega t-(\gamma_a-\gamma_s)t}\sum_{k=1}^{\infty}\left[\frac{-ib}{\pm n\Omega + i(\gamma_a-\gamma_s)}\right]^k j_k(bt), \tag{A8}$$

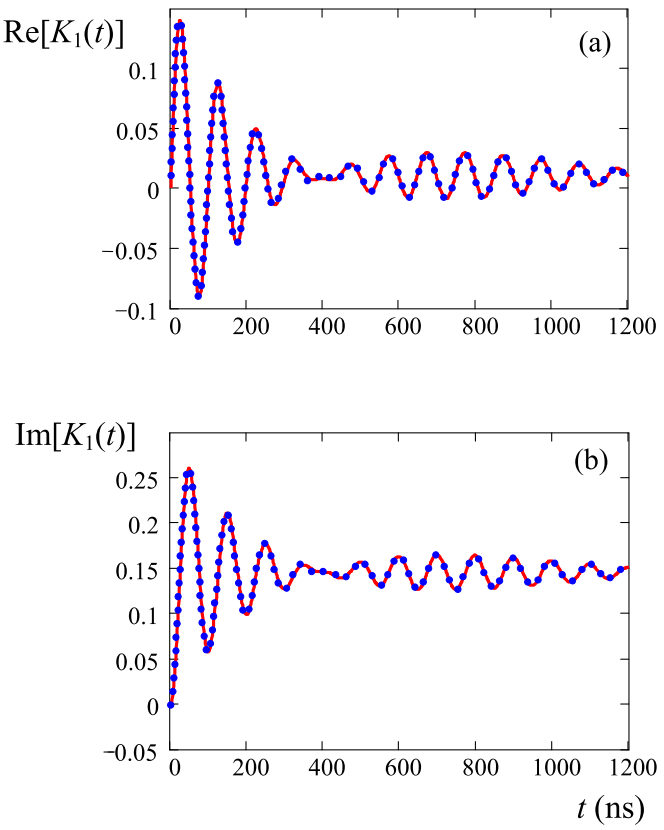

FIG. 11. (Color online) Comparison of the time dependencies of the real (a) and imaginary (b) parts of the integral $K_1(t)$ Eq. (A6) (solid line in red) with Eq. (A7), where only the first term in the sum, Eq. (A8), is taken into account (dotted line in blue). The parameters are $b = 1.47$ MHz and $\Omega = 10$ MHz.

where $j_k(bt) = J_k(2\sqrt{bt})/(bt)^{k/2}$ and $J_k(x)$ is the Bessel function of the kth order. If $n\Omega \gg b$, then the smallness of the satellites' contribution is of the order of $b/n\Omega$. For example, when $b/\Omega = 0.146$, $n = 1$, and $\gamma_a \approx \gamma_b$, then it is already a fine approximation if one takes into account only the first term in the sum $M_{\pm1}(t)$ in Eq. (A8), which is proportional to b/Ω (see Fig. 11).

APPENDIX B

The averaged probability amplitude $\langle P(t-t_0)\rangle_{t_0} = \langle N(t)\rangle$ [Eq. (7)] is described by the equation (see Refs. [33,68])

$$\langle N(t)\rangle = \mathrm{Re}\left\{1 - 2f_s bF_+(t)\int_{-\infty}^{t} dt' j_1[b(t-t')]/F_+(t') + 2f_s b^2 e^{-2\gamma_a t}\int_{-\infty}^{t} dt' F_-(t') j_1[b(t-t')] \times \int_{-\infty}^{t'} dt'' j_1[b(t-t'')]/F_+(t'')\right\}, \tag{B1}$$

where f_s is the recoilless fraction of the source photons and

$$F_\pm(t) = \exp[-(\gamma_s \pm \gamma_a)t - i(\omega_a-\omega_s)t - ip\sin(\Omega t)]. \tag{B2}$$

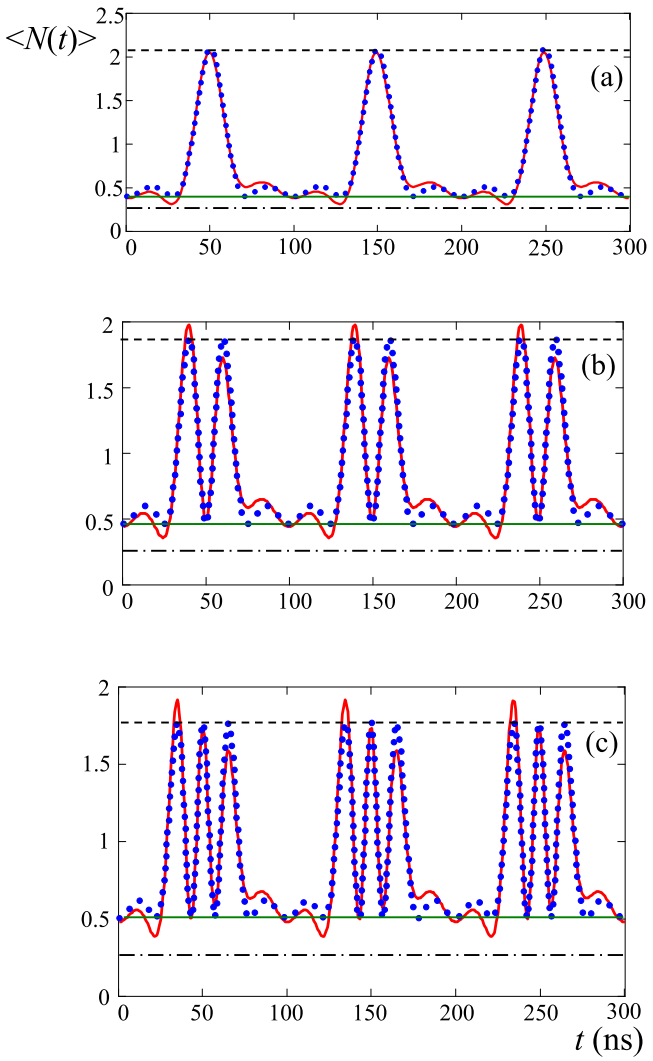

FIG. 12. (Color online) Time dependence of the photon counts, averaged over t_0, for $\Delta = \Omega$ and $p = 1.8$ (a), $\Delta = 2\Omega$ and $p = 3.1$ (b), $\Delta = 3\Omega$ and $p = 4.2$ (c). Solid line (in red) represents the exact result and dotted line (in blue) the analytical approximation (8). Dashed black line shows the level $\langle N_m\rangle_{\max}$, solid line (in green) $\langle N_m\rangle_{\min}$, and dashed-dotted line represents $\langle N\rangle_{\rm res}$. Other parameters are defined in the text.

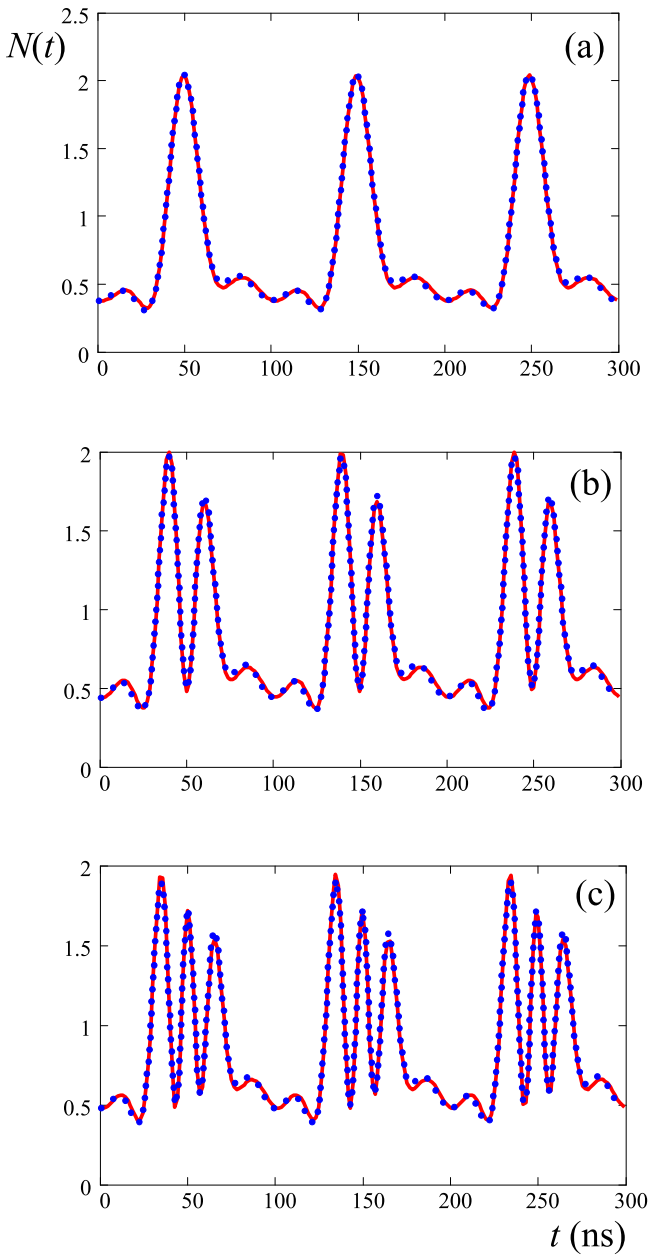

FIG. 13. (Color online) Comparison of the exact result (solid line in red) for time dependence of the photon counts, averaged over t_0, for $\Delta = \Omega$ and $p = 1.8$ (a), $\Delta = 2\Omega$ and $p = 3.1$ (b), $\Delta = 3\Omega$ and $p = 4.2$ (c) with analytical approximation (B7) (dotted line in blue). Other parameters are the same as in Figs. 1(a)–1(c) of the main part of the paper.

If $\gamma_s = \gamma_a = \gamma$, then Eq. (B1) can be simplified as follows:

$$\langle N(t)\rangle = 1 - 2f_s b\int_0^\infty dt' j_1(bt')e^{-2\gamma t'} \times \cos[\phi(t) - \phi(t-t') - \Delta\omega t'] + 2f_s b^2\int_0^\infty dt'\int_0^{t'} dt'' j_1(bt')j_1(bt'')e^{-2\gamma t'} \times \cos[\phi(t-t') - \phi(t-t'') + \Delta\omega(t'-t'')], \quad \text{(B3)}$$

where $\Delta\omega = \omega_s - \omega_a$ is the resonant detuning and $\phi(t) = p\sin(\Omega t + \varphi)$ is the phase modulation of the radiation field in the reference frame of the vibrating absorber.

Equations (B1) and (B3) are hard to analyze analytically. On the contrary, the analytical approximation, given in Eq. (8), helps to estimate the periodicity of pulses, the values of their maxima $\langle N_m\rangle_{\max}$, and the intensity level of the dark windows $\langle N_m\rangle_{\min}$, where index m indicates that the mth component is in resonance. According to the analytical approximation, these values are

$$\langle N_m\rangle_{\max} = [1 + V_m(p)]^2 + J_m^2(p)(\langle N\rangle_{\rm res} - e^{-T_a/2}), \quad \text{(B4)}$$

$$\langle N_m\rangle_{\min} = [1 - V_m(p)]^2 + J_m^2(p)(\langle N\rangle_{\rm res} - e^{-T_a/2}), \quad \text{(B5)}$$

where $\langle N\rangle_{\rm res} = \exp(-T_a/2)I_0(T_a/2)$ is proportional to the number of counts per unit time at the output of the single-line

absorber if it is tuned in resonance with the source. Comparison of the analytical approximation (8), with the exact expression (B3), for the number of counts at the output of the vibrating absorber, is shown in Fig. 12, along with the values $\langle N_m\rangle_{\max}$, $\langle N_m\rangle_{\min}$, and $\langle N\rangle_{\rm res}$, which are $\langle N_1\rangle_{\max}=2.089$, $\langle N_1\rangle_{\min}=0.397$ for $\Delta=\Omega$ and $p=1.8$; $\langle N_2\rangle_{\max}=1.877$, $\langle N_2\rangle_{\min}=0.463$ for $\Delta=2\Omega$ and $p=3.1$; $\langle N_3\rangle_{\max}=1.768$, $\langle N_3\rangle_{\min}=0.504$ for $\Delta=3\Omega$ and $p=4.2$. These values are obtained if modulation frequency is $\Omega=10$ MHz and $T_a=5.2$, when $\langle N\rangle_{\rm res}=0.264$. The maximum intensity of the pulses exceeds almost two times the radiation intensity without absorber. Minimum intensity in the dark windows $\langle N_m\rangle_{\min}$ is almost an order of magnitude smaller than the maximum pulse intensity $\langle N_m\rangle_{\max}$ and slightly exceeds the intensity level of the radiation field, transmitted through the resonant absorber not vibrating $\langle N\rangle_{\rm res}$. However, their difference $\langle N_m\rangle_{\min}-\langle N\rangle_{\rm res}$ rises with increase of the value of the modulation index from $p=1.8$ to 4.2.

It is possible to improve the analytical approximation, given in Eq. (8), if the contribution of two nearest satellites of the resonant component are taken into account, i.e.,

$$a_{\rm apx}(t,l)=a_A(t,l)+a_m(t,l)+a_{m+1}(t,l)+a_{m-1}(t,l). \quad \text{(B6)}$$

In the corresponding probability amplitude $P_{\rm apx}(t)=|a_{\rm apx}(t,l)|^2$ we can make further simplification neglecting the terms $|a_{m+1}(t,l)+a_{m-1}(t,l)|^2$ and $2\,\mathrm{Re}\,\{[a_{m+1}(t,l)+a_{m-1}(t,l)]a_L(t,l)J_0(2\sqrt{bt})e^{im(\Omega t+\varphi)}\}$ since their contribution into the averaged probability $\langle P_{\rm apx}(t-t_0)\rangle_{t_0}$ is small. The contribution of other terms results in the expression

$$\langle N_{\rm apx}(t)\rangle=\langle N_m(t)\rangle-\langle C_{m+1}(t)\rangle-\langle C_{m-1}(t)\rangle, \quad \text{(B7)}$$

where $\langle N_m(t)\rangle=\langle P(t-t_0)\rangle_{t_0}$ is defined in Eq. (8) and

$$\begin{aligned}\langle C_{m\pm1}(t)\rangle &= 2J_{m\pm1}(p)\Big\{\cos\psi_{m\pm1}(t)-e^{-B}\cos[\psi_{m\pm1}(t)\pm D]\\ &\quad -J_m(p)[\cos(\Omega t+\varphi)-e^{-B}\cos(\Omega t+\varphi+D)]\Big\}, \quad \text{(B8)}\end{aligned}$$

$$B+iD=\frac{b}{2\gamma-i\Omega}. \quad \text{(B9)}$$

It is easy to show that the contribution of terms $\langle C_{m\pm1}(t)\rangle$ is as small as $2b\gamma/\Omega^2$ if $\Omega\gg2\gamma$ and $\Omega\gg b$. However, in spite of the smallness of the corrections, Eq. (B7) describes much better the formation of pulses than the analytical approximation (8) (see Fig. 13), where Eq. (B7) is compared with the exact result. Misfit between them is almost negligible.

[1] Yu. Kagan, Hyperfine Interact. **123/124**, 83 (1999).
[2] J. P. Hannon and G. T. Trammell, Hyperfine Interact. **123/124**, 127 (1999).
[3] G. V. Smirnov, Hyperfine Interact. **123/124**, 31 (1999).
[4] G. V. Smirnov, U. van Bürck, J. Arthur, G. S. Brown, A. I. Chumakov, A. Q. R. Baron, W. Petry, and S. L. Ruby, Phys. Rev. A **76**, 043811 (2007).
[5] M. O. Scully, Phys. Rev. Lett. **102**, 143601 (2009).
[6] R. Röhlsberger, K. Schlage, B. Sahoo, S. Couet, and R. Rüffer, Science **328**, 1248 (2010).
[7] J. Amann *et al.*, Nat. Photonics **6**, 693 (2012).
[8] Yu. Svyd'ko, S. Stoupin, V. Blank, and S. Terentyev, Nat. Photonics **5**, 539 (2011).
[9] J. Chen, I. V. Tomov, A. O. Er, and P. M. Rentzepis, Appl. Phys. Lett. **102**, 174101 (2013).
[10] R. Röhlsberger, H.-C. Wille, K. Schlage, and B. Sahoo, Nature (London) **482**, 199 (2012).
[11] F. Döring, A. L. Robisch, C. Eberl, M. Osterhoff, A. Ruhlandt, T. Liese, F. Schlenkrich, S. Hoffmann, M. Bartels, T. Salditt, and H. U. Krebs, Opt. Express **21**, 019311 (2013).
[12] T. Osaka, M. Yabashi, Y. Sano, K. Tono, Y. Inubushi, T. Sato, S. Matsuyama, T. Ishikawa, and K. Yamauchi, Opt. Express **21**, 2823 (2013).
[13] B. W. Adams *et al.*, J. Mod. Opt. **60**, 2 (2013).
[14] F. Vagizov, V. Antonov, Y. V. Radeonychev, R. N. Shakhmuratov, and O. Kocharovskaya, Nature (London) **508**, 80 (2014).
[15] W.-T. Liao, A. Pálffy, and C. H. Keitel, Phys. Rev. Lett. **109**, 197403 (2012).
[16] W.-T. Liao and A. Pálffy, Phys. Rev. Lett. **112**, 057401 (2014).
[17] K. P. Heeg, H.-C. Wille, K. Schlage, T. Guryeva, D. Schumacher, I. Uschmann, K. S. Schulze, B. Marx, T. Kämpfer, G. G. Paulus, R. Röhlsberger, and J. Evers, Phys. Rev. Lett. **111**, 073601 (2013).
[18] K. P. Heeg *et al.*, Phys. Rev. Lett. **114**, 203601 (2015).
[19] L. A. Rivlin, Quantum Electron. **37**, 723 (2007).
[20] N. Gisin, G. Ribordy, W. Tittel, and H. Zbinden, Rev. Mod. Phys. **74**, 145 (2002).
[21] A. I. Lvovsky, B. C. Sanders, and W. Tittel, Nat. Photonics **3**, 706 (2009).
[22] J. Brendel, N. Gisin, W. Tittel, and H. Zbinden, Phys. Rev. Lett. **82**, 2594 (1999).
[23] I. Marcikic, H. de Riedmatten, W. Tittel, V. Scarani, H. Zbinden, and N. Gisin, Phys. Rev. A **66**, 062308 (2002).
[24] R. T. Thew, A. Acin, H. Zbinden, and N. Gisin, Phys. Rev. Lett. **93**, 010503 (2004).
[25] B. R. Nisbet-Jones, J. Dilley, A. Holleczek, O. Barter, and A. Kuhn, New J. Phys. **15**, 053007 (2013).
[26] P. Kolchin, C. Belthangady, S. Du, G. Y. Yin, and S. E. Harris, Phys. Rev. Lett. **101**, 103601 (2008).
[27] Yu. V. Svyd'ko, S. L. Popov, and G. V. Smirnov, Pis'ma Zh. Eksp. Teor. Fiz. **53**, 217 (1991) [JETP Lett. **53**, 231 (1991)]; J. Phys.: Condens. Matter **5**, 1557 (1993).
[28] Yu. V. Shvyd'ko, T. Hertrich, U. van Bürck, E. Gerdau, O. Leupold, J. Metge, H. D. Rüter, S. Schwendy, G. V. Smirnov, W. Potzel, and P. Schindelmann, Phys. Rev. Lett. **77**, 3232 (1996).
[29] A. Palffy, C. H. Keitel, and J. Evers, Phys. Rev. Lett. **103**, 017401 (2009).
[30] P. Helisto, I. Tittonen, M. Lippmaa, and T. Katila, Phys. Rev. Lett. **66**, 2037 (1991).
[31] I. Tittonen, M. Lippmaa, P. Helisto, and T. Katila, Phys. Rev. B **47**, 7840 (1993).

[32] P. Helisto, E. Ikonen, T. Katila, W. Potzel, and K. Riski, Phys. Rev. B **30**, 2345 (1984).
[33] E. Ikonen, P. Helisto, T. Katila, and K. Riski, Phys. Rev. A **32**, 2298 (1985).
[34] P. Schindelmann, U. van Bürck, W. Potzel, G. V. Smirnov, S. L. Popov, E. Gerdau, Yu. V. Shvyd'ko, J. Jäschke, H. D. Rüter, A. I. Chumakov, and R. Rüffer, Phys. Rev. A **65**, 023804 (2002).
[35] R. N. Shakhmuratov, F. Vagizov, and O. Kocharovskaya, Phys. Rev. A **84**, 043820 (2011).
[36] R. N. Shakhmuratov, F. G. Vagizov, and O. A. Kocharovskaya, Bull. Russ. Acad. Sci.: Phys. **76**, 248 (2012).
[37] R. N. Shakhmuratov, F. Vagizov, and O. Kocharovskaya, Phys. Rev. A **87**, 013807 (2013).
[38] R. N. Shakhmuratov, F. G. Vagizov, and O. A. Kocharovskaya, Bull. Russ. Acad. Sci.: Phys. **78**, 199 (2014).
[39] G. V. Smirnov, U. van Bürck, J. Arthur, S. L. Popov, A. Q. R. Baron, A. I. Chumakov, S. L. Ruby, W. Potzel, and G. S. Brown, Phys. Rev. Lett. **77**, 183 (1996).
[40] R. N. Shakhmuratov, Phys. Rev. A **85**, 023827 (2012).
[41] F. J. Lynch, R. E. Holland, and M. Hamermesh, Phys. Rev. **120**, 513 (1960).
[42] B. Lounis and W. E. Moerner, Nature (London) **407**, 491 (2000).
[43] S. M. Harris, Phys. Rev. **124**, 1178 (1961).
[44] M. D. Crisp, Phys. Rev. A **1**, 1604 (1970).
[45] R. N. Shakhmuratov, F. Vagizov, J. Odeurs, and O. Kocharovskaya, Phys. Rev. A **80**, 063805 (2009).
[46] R. N. Shakhmuratov, Phys. Rev. A **90**, 013819 (2014).
[47] C. W. Hillegas, J. X. Tull, D. Goswami, D. Strickland, and W. S. Warren, Opt. Lett. **19**, 737 (1994).
[48] M. R. Fetterman, D. Goswami, D. Keusters, W. Yang, J.-K. Rhee, and W. S. Warren, Opt. Express **3**, 366 (1998).
[49] T. E. Cranshaw and P. Reivari, Proc. Phys. Soc., London **90**, 1059 (1967).
[50] S. L. Ruby and D. I. Bolef, Phys. Rev. Lett. **5**, 5 (1960).
[51] G. Kornfeld, Phys. Rev. **177**, 494 (1969).
[52] J. Mishroy and D. I. Bolef, in *Mössbauer Effect Methodology*, edited by I. J. Gruverman (Plenum, New York, 1968), Vol. 4, p. 13.
[53] C. L. Chein and J. C. Walker, Phys. Rev. B **13**, 1876 (1976).
[54] A. R. Mkrtchyan, A. F. Arakelyan, and L. A. Kocharyan, Pis'ma Zh. Eksp. Teor. Fiz. **26**, 599 (1977) [JETP Lett. **26**, 449 (1977)].
[55] G. J. Perlow, Phys. Rev. Lett. **40**, 896 (1978).
[56] J. E. Monahan and G. J. Perlow, Phys. Rev. A **20**, 1499 (1979).
[57] A. R. Mkrtchyan, G. A. Arutyunyan, A. R. Arakelyan, and R. G. Gabrielyan, Phys. Status Solidi B **92**, 23 (1979).
[58] L. T. Tsankov, J. Phys. A: Math. Gen. **14**, 275 (1981).
[59] S. L. Popov, G. V. Smirnov, and Y. V. Shvyd'ko, Pis'ma Zh. Eksp. Teor. Fiz. **49**, 651 (1989) [JETP Lett. **49**, 747 (1989)].
[60] Y. V. Svyd'ko and G. V. Smirnov, J. Phys.: Condens. Matter **4**, 2663 (1992).
[61] A. Nazarkin, G. Korn, M. Wittmann, and T. Elsaesser, Phys. Rev. Lett. **83**, 2560 (1999).
[62] S. M. Cavaletto, Z. Harman, C. Ott, C. Buth, T. Pfeifer, and C. H. Keitel, Nat. Photonics **8**, 520 (2014).
[63] K. Krajewska, M. Twardy, and J. Z. Kaminski, Phys. Rev. A **89**, 032125 (2014).
[64] Y. V. Radeonychev, V. A. Polovinkin, and O. Kocharovskaya, Phys. Rev. Lett. **105**, 183902 (2010).
[65] V. A. Antonov, Y. V. Radeonychev, O. Kocharovskaya, Phys. Rev. A **88**, 053849 (2013).
[66] D. C. Burnham and R. Y. Chao, Phys. Rev. **188**, 667 (1969).
[67] E. Varoquaux, G. A. Williams, and O. Avenel, Phys. Rev. B **34**, 7617 (1986).
[68] E. Kuznetsova, R. Kolesov, and O. Kocharovskaya, Phys. Rev. A **68**, 043825 (2003).